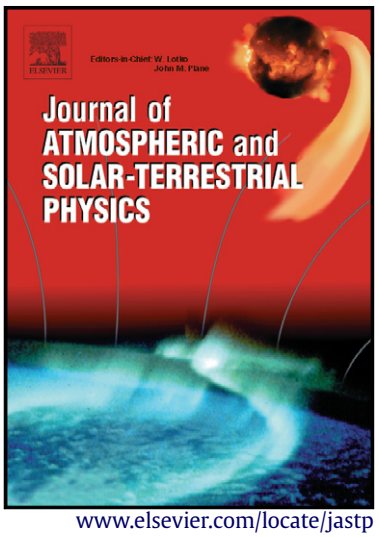

www.elsevier.com/locate/jastp

Assessing the GNSS scintillation climate over Brazil under increasing solar activity

Luca Spogli, Lucilla Alfonsi, Vincenzo Romano, Giorgiana De Franceschi, Joao FranciscoGalera Monico , Milton Hirokazu Shimabukuro, Bruno Bougard, Marcio Aquino

PII: S1364-6826(13)00260-5
DOI: http://dx.doi.org/10.1016/j.jastp.2013.10.003
Reference: ATP3922

To appear in: *Journal of Atmospheric and Solar-Terrestrial Physics*

Received date: 26 October 2012
Revised date: 16 September 2013
Accepted date: 3 October 2013

Cite this article as: Luca Spogli, Lucilla Alfonsi, Vincenzo Romano, Giorgiana De Franceschi, Joao FranciscoGalera Monico , Milton Hirokazu Shimabukuro, Bruno Bougard, Marcio Aquino, Assessing the GNSS scintillation climate over Brazil under increasing solar activity, *Journal of Atmospheric and Solar-Terrestrial Physics,* http://dx.doi.org/10.1016/j.jastp.2013.10.003

Assessing the GNSS scintillation climate over Brazil under increasing solar activity

Luca Spogli[1], Lucilla Alfonsi[1], Vincenzo Romano[1,4], Giorgiana De Franceschi[1], Joao Francisco Galera Monico[2], Milton Hirokazu Shimabukuro[2], Bruno Bougard[3], Marcio Aquino[4]

[1]Istituto Nazionale di Geofisica e Vulcanologia, Italy

[2]Universidade Estadual Paulista "Jùlio de Mesquita Filho", Brazil

[3]Septentrio Satellite Navigation, Belgium

[4]University of Nottingham, United Kingdom

Corresponding author:

Luca Spogli

email: luca.spogli@ingv.it

tel: +39 06 5186 0609

fax: +39 06 5186 0397

Abstract

We study ionospheric scintillation on GNSS signals at equatorial latitudes to draw a climatological picture of the low latitude ionosphere in the Brazilian sector during the ascending phase of the upcoming 2013 solar maximum. Such data have been acquired during the early stage of the CIGALA project (http://cigala.galileoic.org/), funded by the European Commission under the 7th Framework Program and the outcome of this work is part of the scientific achievements of the project itself. The considered network is based on the novel PolaRxS receivers, developed and deployed specifically to comply with the aims of the FP7 project. The PolaRxS is able to monitor ionospheric scintillation for all operational and upcoming GNSS constellations (GPS, GLONASS, Compass, GALILEO) and corresponding frequencies in the L-band. The ionosphere over the Brazilian territory, being close to the southern crest of the Equatorial Ionospheric Anomaly (EIA), is heavily affected by intense scintillation conditions. The sector under investigation is also very peculiar with respect to other low latitude regions, because of its proximity to the South Atlantic Magnetic Anomaly (SAMA). The application of the Ground Based Scintillation Climatology (GBSC) technique, for the first time simultaneously on GPS and GLONASS data and on both L1 and L2 frequencies, highlights the joint effect of the EIA and of the SAMA in producing the irregularities leading to scintillation.

1. Introduction

The ionosphere in the latitudinal sector between -20°N to +20°N degrees is a preferred site for hosting ionospheric irregularities driving scintillation phenomena during the local post-sunset hours. Ionospheric scintillation is characterized by sudden, rapid fluctuations of the trans-ionospheric signal carrier frequency recorded at ground level. It occurs mainly at equatorial and polar latitudes and varies on large time and space scale ranges. At equatorial latitudes, where the phenomenon is stronger, the induced fading can exceed 20 dB (Basu et al., 2002), jeopardizing, for instance, all current technologies relying on GNSS (Global Navigation Satellite System) precise positioning, such as navigation, precision agriculture, safety of life, etc.

The strength of the scintillations at low latitude is due to the morphology of the equatorial ionosphere that is very peculiar with respect to other latitudes. In fact, at the magnetic equator, the B field is parallel to the Earth surface and produces the so-called “fountain effect”: an ionospheric plasma movement upward and downward, due to the interplay among ExB drift, gravity and pressure gradients. This mechanism leads to the formation of the EIA, with minimum F-region ionization density at the magnetic equator and maxima at the two crests, which are located roughly at 20° in magnetic latitude northward and southward. Even if the decreasing of the sun forcing after

the local sunset leads to weakening of the equatorial anomaly, at this time a dynamo develops in the F-region due to polarization charges within conductivity gradients at the terminator. Moreover, such currents are no longer subject to the shorting effect of the conducting E-layer to the north and south of the magnetic equator. Polarization fields are thus able to drive the F-layer upwards and, when the electric field eventually turns westward, the plasma starts to drift downward. The overall effect is that the field is much enhanced just after the sunset (Rishbeth, 1971). This is called the post-sunset or the pre-reversal enhancement of the eastward electric field. This configuration leads to the formation a Rayleigh–Taylor instability (e.g. Jin et al., 2008) which allows the formation of ionospheric irregularities, mainly large electron density depletions elongated along the magnetic lines often called "plasma bubbles" (see, e.g., Young et al, 1984). At low latitudes, the small-scale irregularities embedded in the plasma bubbles are amongst the most challenging for the reliability of trans-ionospheric signals (Wernik and Liu, 1974). They can cause strong scintillation and therefore severe degradation of the accuracy of the signal phase measurements from several satellites simultaneously, which may preclude positioning.

Moreover, the whole Brazilian sector is characterized by the presence of the South Atlantic Magnetic Anomaly (SAMA) that is a large anomaly of the Earth's magnetic field, covering most of the South Atlantic, from West Africa to South America and from the equator to Antarctica. The SAMA is characterized by the lowest values of the geomagnetic field intensity at the Earth's surface and, consequently, by enhanced particle radiation flux at middle latitudes coming into the atmosphere (Abdu et al., 2005). Particle precipitation in the SAMA is a source of ionospheric turbulence leading to scintillation, similar to what happens in the cusp at polar latitude. It disturbs the thermospheric circulation in the atmosphere and alters the rates of production and recombination of the ionized species, mainly during geomagnetic storms.

A deep study of the low latitude ionosphere is important both for the understanding of physical mechanisms involved in the formation of the ionospheric plasma irregularities and for the mitigation of the impact they have on trans-ionospheric signals, mainly those of GNSS satellites. This is particularly true in an area as populated as Brazil, and Latin America in general.

To face the challenge of the resilience of GNSS signals to the next 2013 solar maximum, the CIGALA project (http://cigala.galileoic.org/) has been conceived and funded under the EU Seventh Framework Program. It was carried out in the context of the Galileo 7th FP R&D program supervised by the European GNSS Agency from March 2010 to February 2012. CIGALA aimed to develop and test ionospheric scintillation mitigation approaches over Latin America to be implemented in professional multi-frequency multi-GNSS receivers, developed *ad-hoc* and named PolaRxS. In order to achieve this, the project leveraged research and development activities

coordinated between leading European and Brazilian experts and set up a wide-scale measurement and test campaign at several locations in Brazil during the period of increasing solar activity.

In the framework of the project, the Ground Based Scintillation Climatology (GBSC) technique (Spogli et al, 2009, 2010; Alfonsi et al., 2010) is applied to CIGALA field data and historical data for a climatological representation of ionospheric scintillation, aiming to identify the areas of the ionosphere and the times of the day in which the phenomenon is most likely to occur.

Most of the recent literature about the Brazilian ionosphere describe the perturbed conditions resulting from electron density irregularities which drive scintillations on trans-ionospheric satellite signals. Such investigations are supported by case events (see, e.g., Abdu et al., 2002) or by climatological studies mainly conducted on GPS only and by means of single frequency receivers (like the SCINTMON), as in Muella et al. (2008 and 2010). These studies clearly demonstrate the peculiarity of the Brazilian ionosphere in producing scintillation-effective irregularities. This work extends the prior work through the novelty of a climatological representation of the Brazilian ionosphere by means of a multi-constellation dataset (GPS and GLONASS) on both L1 and L2 frequencies. The observations cover a sufficiently large part of the Brazilian ionosphere to provide evidence of the contributions of both EIA and SAMA in producing irregularities in the Brazilian ionosphere.

By highlighting the similarities and differences among the data from the two constellations, a more robust mapping is presented herein, especially due to the wider field of view coverage. Moreover, the differences between scintillation on L1 and L2 signals are shown in a climatological representation.

The paper is organized as follows: section 2 introduces the scintillation data used in the present analysis. The section is organized in 2 subsections: the first one presents the Septentrio PolaRxS data, and the second one the historical data acquired by a SCINTMON receiver. Section 3 presents the main features of GBSC, the technique adopted to analyse data. In section 4 the main results are presented, while the conclusions and remarks are in section 5.

2. Data

PolaRxS data

The PolaRxS is a multi-frequency, multi-constellation receiver capable of tracking simultaneously GPS L1CA, L1P, L2C, L2P, L5; GLONASS L1CA, L2CA; Galileo E1, E5a, E5b, E5AltBoc; COMPASS B1, B2; SBAS L1 (Bougard et al, 2011). Sampling at 50 Hz, the receiver gives the following main output parametetrs:

1. the σ_{Φ} phase scintillation index calculated over different time intervals (1, 3, 10, 30, 60 seconds);
2. the S_4 amplitude scintillation index calculated over 60 seconds;
3. the Total Electron Content (TEC) and the Rate of TEC change (ROT) every 15 seconds,
4. the spectral parameters: spectral slope of the phase Power Spectral Density (p) in the 0.1 to 25 Hz range and the spectral strength of the phase PSD (T) at 1 Hz (60 seconds);
5. the Standard Deviation of the Code Carrier (CCSTDDEV - 60 seconds) ;
6. the Average Carrier to noise (Cn) ratio (60 seconds);
7. locktime (60 seconds).

All these quantities (except TEC and ROT) are calculated for all the available signal frequencies emitted by the satellites and along the slant path receiver - satellite. TEC values are obtained by the pseudorange measurements only. For GPS, the TEC is based on the L2-P and L1-P pseudoranges; for GLONASS it is based on the L1-C/A and L2-C/A pseudoranges and for Galileo, it is based on the L1BC and E5a. ROT is computed from the carrier phase measurements only, and hence is much more accurate than TEC.

The receivers have been deployed during the early stage of the project at selected Brazilian sites, shown in Figure 1. Receiver IDs, locations, geographic coordinates, geomagnetic latitude, and installation date are summarized in Table 1. Locations have been chosen to satisfy scientific and practical issues, such as:

- Meaningful spread in geographic Latitude and Longitude to cover the widest portion of ionosphere;
- Possible co-location with other instruments (e.g. Ionosondes are present in MANA, PALM, SJCU, SJCI);
- Low multipath/noise environment and good antenna sky visibility;
- Power network stability and
- Internet connection bandwidth and stability for data transfer to the central repository.

Data used for the analysis of the CIGALA network refers to August-November 2011, which has been considered to be meaningful to catch the scintillation recurrent features in the ionosphere during the rising phase of the solar maximum, including also the effect due to the equinox. Moreover, in this period 7 out of 8 CIGALA receivers were operative and collected data simultaneously. Table 2 summarizes the percentage of available days of data for each receiver in the considered period. Except for PRU1 receiver (48.4%), which is almost co-located with PRU2

(distance 300m), all the data availability is good enough to have comparable statistics to produce climatological maps, as described in section 3.

SCINTMON data

Historical GPS data acquired by a SCINTMON receiver (SCINTillation MONitor receiver, http://gps.ece.cornell.edu/rxdesign.php) located in Presidente Prudente have been used to test and compare with CIGALA network data by using the GBSC technique. The SCINTMON receiver is managed by the Instituto Nacional de Pesquisas Espaciais (INPE), which has the ownership of the data. The SCINTMON receiver was originally developed by Cornell University and is composed of Zarlink GPS chip sets that perform the fast digital functions, such as PRN code correlation, and software running on a PC in an open architecture environment to execute the acquisition and tracking loops. The L1 signal amplitude is computed at 50 Hz. Typically 10 channels of the SCINTMON receiver are devoted to GPS signals, one channel is devoted to a WAAS signal, and one channel is detuned to measure noise. The first 11 channels are compared to the noise channel to compute the carrier-to-noise ratios and the amplitude scintillation index S_4 is computed by taking the ratio of the standard deviation of Cn to the mean of Cn over a one minute period (http://gps.ece.cornell.edu/realtime.php). S_4 data of the SCINTMON in Presidente Prudente presented here refer to year 2009, from Jan 1st to Oct 31st, with a significant data gap between Jun 29th and Jul 25th, under low solar activity conditions. The receiver has been set to acquire data only during the time range 2100 UT to 0900 UT, corresponding to 1800 LT to 0600 LT, in order to observe the effect of the EIA. To compare with SCINTMON data, the sole contribution of PRU1 and PRU2 CIGALA receivers from February to October 2011 is considered to make the two datasets as much consistent as possible, keeping in mind the very different helio-geophysical conditions of the two considered periods (2009 vs. 2011).

3. Method

GBSC has been recently developed (Spogli et al, 2009, 2010; Alfonsi et al., 2011) as a tool to identify the main areas of the ionosphere in which ionospheric scintillation is more likely to occur. GBSC relies on the internationally adopted phase and amplitude scintillation indices σ_Φ and S_4, respectively, and was originally developed for GPS data collected at high latitudes, to investigate the physical process involved in the scintillation phenomena. The aim was also to contribute to mitigation algorithms and as a first step towards the forecasting of Space Weather related events with GNSS receivers. At the core of the GBSC are the maps of the mean values, standard deviations and percentages of occurrence above arbitrary threshold of the parameters output by the receiver, mainly the scintillation indices. The coordinates system can be selected in terms of pairs of the following: geographic coordinates (latitude and longitude), altitude adjusted geomagnetic

coordinates (magnetic latitude and magnetic longitude), universal time, magnetic local time, azimuth and elevation. The percentage of occurrence O is evaluated in each bin of the map according to the following definition:

$$O=\frac{N_{thr}}{N_{tot}}, \qquad (1)$$

where N_{thr} is the number of data points corresponding to the investigated scintillation index above a given threshold and N_{tot} is the total number of data points in the bin. Thresholds are chosen in order to distinguish between different scintillation scenarios: for moderate/strong scintillation, typical threshold values are 0.25 radians for σ_Φ and 0.25 for S_4, while for weak scintillation conditions, threshold values are 0.1 radians and 0.1, respectively. In order to reduce the impact of non-scintillation related tracking errors (such as multipath) only indices computed from observations at elevation angles α_{elev}, as calculated from the receiver to the selected satellite, greater than 20° are considered. Scintillation indices are projected to the vertical, in order to account for varying geometrical effects on the measurements made at different elevation angles, as in the following formulae:

$$\sigma_\Phi^{vert} = \frac{\sigma_\Phi^{slant}}{(F(\alpha_{elev}))^{\frac{1}{2}}}, \qquad (2)$$

$$S_4^{vert} = \frac{S_4^{slant}}{(F(\alpha_{elev}))^{\frac{p+1}{4}}}, \qquad (3)$$

where σ_Φ^{slant} and S_4^{slant} are the indices directly measured at a given elevation angle along the slant path. In the two formula above, $F(\alpha_{elev})$ is the obliquity factor, that is defined as (Mannucci et al., 1993):

$$F(\alpha_{elev}) = \frac{1}{\sqrt{1-\left(\frac{R_E \cos \alpha_{elev}}{R_E+H_{IPP}}\right)^2}}, \qquad (4)$$

where R_E is the Earth radius and H_{IPP} is the height of the Ionospheric Piercing Point, assumed to be 350 km and p is the phase spectral slope, directly measured by PolaRxS. If p is not measured, as for SCINTMON data, according to Rino (1979) and as described in Spogli et al. (2009), the exponent p is chosen to be p=2.6, from which $\frac{p+1}{4} = 0.9$. However, slight differences on this assumption do not have a meaningful impact on a statistical representation of large datasets. The binning can be selected, typically according to the available statistics and to obtain a meaningful fragmentation of the map.

The angular dependence of the scintillation indices in the formula (2) and (3) is valid only under the conditions of weak scattering and when single phase screen approximation is suitable. However, we decided to apply the formula for weak scattering also to characterize the moderate/strong scintillation regime for the following reasons:

1) The nature of this study is statistical and its aim is to identify climatological patterns of scintillation in terms of occurrence above the aforementioned thresholds. Bearing this in mind, the risk to apply the weak formula to the moderate/strong regime is reduced in our approach to an underestimation of the occurrence. In fact, the projection to the vertical through equations (19) and (31) of the paper by Rino (1979) leads to a smaller value of the given slant index. This implies an underestimation of the corresponding occurrence when calculated with vertical values. This is an intrinsic limitation of the GBSC approach, affecting mainly values near 0.25 (radians), i.e. values corresponding to moderate scattering, that can fall below the occurrence threshold if projected to the vertical. This could be limiting in case one would separate moderate and strong scintillation regimes and will be taken into account in further releases of the GBSC.
2) The GBSC aims to represent the scintillation environment in the considered area in a way as much as possible independent on the locations of the receivers. In this sense, formula (2) and (3) address the need to avoid geometrical effects on the results.

The GBSC technique, originally developed for GISTM (GPS Ionospheric Scintillation and TEC Monitor, Van Dierendonck, 1993) receivers and for high latitude, has been adapted within CIGALA to the scope of the project. In particular it was first implemented for the archive data of the Presidente Prudente SCINTMON and then extended to accept the input of PolaRxS data.

4. Results

Figure 2 shows the map of S_4 percentage of occurrence above 0.25 (moderate/strong scattering characterization) in geographic coordinates for GPS L1 frequency in the considered period (August to November 2011). It is observed that a slight enhancement of scintillation occurrence (<10%) is distributed in a band almost parallel to the geomagnetic equator. This is the signature of the post sunset scintillation likely due to the southern crest of the EIA. Moreover a strong enhancement of

scintillation occurrence (up to about 20%) has been identified in the region over POAL likely due to the SAMA. Figure 3 shows the map of σ_Φ percentage of occurrence above 0.25 radians (moderate/strong scattering characterization) in geographic coordinates. The occurrence of σ_Φ is lower than the occurrence of S_4 even though, as in the case of S_4, the σ_Φ occurrence is enhanced in a band nearly parallel to the geomagnetic equator. The SAMA seems to not produce any phase scintillation, as opposed to what has been found in the case of amplitude scintillation. However a study over a longer period and the inclusion of mid latitude receivers are necessary for a more accurate characterization of the SAMA effect on GNSS signals.

Figure 4 and Figure 5 show the map of S_4 occurrence above 0.25 and σ_Φ above 0.25 radians (moderate/strong scintillation regime), respectively, in latitude vs. UT. Both amplitude and phase scintillation occurrence are enhanced in the latitudinal range 12°S to 26°S during the post sunset (22 to 04 UT, corresponding to 19 to 01 LT), clearly identifying the EIA scintillation effect. Moreover, the amplitude scintillation around 30°S has only a small dependence on time, reinforcing the idea of the different nature of that enhancement with respect to the one induced by the post sunset effect. Such effect is not present in the phase scintillation occurrence map.

Figure 6 and Figure 7 show the same maps as Figure 2 and Figure 4, but obtained by applying the GBSC to GLONASS L1 data. Both GPS and GLONASS plots clearly show the enhancement of amplitude scintillation due to EIA and SAMA, even if with some minor differences from the quantitative point of view. S_4 data measured with both the GPS and GLONASS constellations can be merged to significantly increase the observability of S_4 is space, time and frequency. The phase scintillation index σ_Φ (not shown here) cannot directly be measured from single frequency GLONASS observations because of the intrinsic jitter of the GLONASS satellite clocks. This effect can however be cancelled out by combining the measurements from both L1 and L2, as all GLONASS satellites provide civilian signals on both carriers (Bougard et al, 2011).

Figure 8 shows the maps of S_4 occurrence above 0.25 in latitude vs. UT for the period August to November 2011 obtained by merging both GPS and GLONASS data. Top plot is for L1, while bottom is for L2 data. Comparing the two maps, it becomes evident that both L1 and L2 highlight the same critical areas of the ionosphere producing scintillation (due to EIA and SAMA), despite the fact that the percentage occurrence is larger for the L2 signal. This is mainly due to the dispersive properties of the ionospheric plasma and also to the different signal to noise ratio, being smaller for L2, as it is transmitted by the satellites with 1.5 dB less power than the L1CA signal. Moreover, only the pilot is used to generate the code and carrier measurement, leading to an extra loss of 3 dB (Bougard et al., 2011).

By applying GBSC on CIGALA data, it can be concluded that S_4 data measured with both GPS and GLONASS constellations can be merged to significantly increase the observability of S_4 in space, time and frequency. Moreover, the application of GBSC on such a large dataset highlights the joint effect of the EIA and of the SAMA in producing the irregularities leading to scintillation scenarios. Also the difference between scintillation on L1 and L2 signals has become evident from the analyses.

Historical data analysis

Figure 9 shows the maps of the percentage of occurrence of S_4>0.1 (weak scintillation characterization) for the above mentioned periods of SCINTMON 2009 (top plot) and PolaRxS GPS 2011 L1 (bottom plot) in the considered periods. Maps are shown as contour plots (the two maps have different scales on the z-axis). Both maps provide evidence of two scintillating areas of the ionosphere in the field of view of the receiver(s): one due to the southern crest of the EIA, where post sunset scintillation is more likely to occur, and another due to the SAMA. The region of enhanced scintillation during the post sunset in 2011 involves a broader latitudinal range (from -14°N to -22°S) than in 2009 data (from -16°N to -20°N). The difference among the two plots in terms of percentage occurrence distribution and values is due to the different solar activity phases considered. In fact, 2009 was a year of solar minimum, while 2011 is on the rising phase of the solar activity. In particular the occurrences measured by PolaRxS in 2011 are almost twice those measured by SCINTMON in 2009 (scales on z axis are different).

5. Conclusions

In this paper, 4 months of ionospheric scintillation data acquired by the PolaRxS receivers of the CIGALA network are analyzed. The data are from August to November 2011, a year of increasing solar activity. Then, 10 months of data collected in one the CIGALA sites, Presidente Prudente (2 receivers, IDs: PRU1 and PRU2), are tested against historical data acquired at the same site by a SCINTMON receiver in 2009. Both PolaRxS and SCINTMON data are represented and interpreted by applying the Ground Based Scintillation Climatology, a technique which is able to identify the recurrent features of ionospheric scintillation in different coordinate systems on large datasets. Although the underestimation of the percentage of occurrence due to the application of the formula (2) and (3) and the limitations of the single phase screen/weak scatter approximation, which remain intrinsic limitations of the GBSC approach, the method is able to show the interesting features of the low latitude ionosphere. As the PolaRxS is a multi-frequency multi-constellation receiver, besides GPS, also GLONASS data are analyzed by means of the GBSC, to investigate the possibility of merging the information coming from the two main constellations to enlarge the field of view and improve the statistics by providing more data over the selected period. GBSC maps in

geographic coordinates and in latitude vs. UT highlight the most critical areas of the ionosphere for both amplitude and phase scintillation. They also provide evidence of the joint effect of EIA and SAMA for irregularities which are scintillation-effective. Moreover the difference between the amplitude scintillation patterns for L1 and L2 signals is considered and presented. S_4 occurrence maps from GPS and GLONASS are in good agreement, while this is not the case for σ_Φ. This is due to the difficulty in identifying phase scintillation from single-frequency GLONASS carrier phase data. The reason for this is that the short-term stability of the GLONASS satellite clocks is lower than that of the GPS satellite clocks. S_4 data measured with both GPS and GLONASS constellations are merged and the GBSC maps are presented for L1 and L2 signals. L1 and L2 scintillation patterns highlight the same critical areas of the ionosphere in producing amplitude scintillation (EIA and SAMA), even if the percentage occurrence is larger for L2 signal, due to the different signal to noise ratios.

The comparative study with SCINTMON historical data shows a good agreement between the two datasets, which are able to draw a similar climatological picture of the scintillation phenomena, albeit with differences due to the contrasting helio-geophysical conditions of the two periods, i.e. 2009 and 2011.

Acknowledgements

The CIGALA project is funded under the EU Seventh Framework Program, and is carried out in the context of the Galileo FP7 R&D program supervised by the GSA. Two monitoring stations were provided by the UNESP foundation (FAPESP) (Processo 2006/04008-2). The authors also want to thank the UNESP complimentary partners in Brazil (IFTO, UFRGS, INPE, UNIVAP, Petrobras, UEA/INPA). The authors would like to thank the Brazilian Instituto Nacional de Pesquisas Espaciais (INPE) for the SCINTMON historical data used here. Research in support of this paper at Nottingham University is funded by the UK Engineering and Physical Sciences Research Council (EPSRC).

References

Abdu, M. A., Batista, I. S., Takahashi, H., MacDougall, J., Sobral, J. H., Medeiros, A. F., Trivedi, N. B., 2002. Magnetospheric disturbance induced equatorial plasma bubble development and dynamics: a case study in Brazilian sector. J. Geophys. Res., 108(A12), 1449, 2003; doi:10.1029/2002JA009721.

Abdu, M.A., Batista, I.S., Carrasco, A.J., and Brum, C.G.M., 2005. South Atlantic magnetic anomaly ionization: A review and a new focus on electrodynamic effects in the equatorial ionosphere. J. Atm. Sol. Terr. Phys. 67, 1643–1657.

Alfonsi, L., Spogli, L., De Franceschi, G., Romano, V., Aquino, M., Dodson, A. Mitchell, C.N., 2011. Bipolar climatology of GPS ionospheric scintillation at solar minimum. Radio Sci., 46, RS0D05, DOI: 10.1029/2010RS004571.

Badhwar, G.D., 1997. Drift rate of the South Atlantic Anomaly. J Geophys Res 102, A2: 2343–2349.

Basu, S., Groves, K.M., Basu, S., Sultan, P.J., 2002. Specification and forecasting of scintillations in communication/navigation links: Current status and future plans. J. Atmos. Sol. Terr. Phys., 64, 1745–1754.

Bougard, B., Sleewaegen, J.-M., Spogli, L., Sreeja, V. V., Galera Monico, J.F., 2011. CIGALA: Challenging the Solar Maximum in Brazil with PolaRxS. Proceeding of the ION GNSS 2011, Portland, Oregon.

Jin, S.G., Luo, O., Park, P., 2008. GPS observations of the ionospheric F2-layer behavior during the 20th November 2003 geomagnetic storm over South Korea. J. Geod. 82 (12), 883–892, doi:10.1007/s00190-008-0217-x.

Mannucci, A.J., Wilson, B.D., Edwards, C.D., 1993. A new method for monitoring the Earth ionosphere total electron content using the GPS global network. Proceedings of ION GPS-93, pp.1323–1332.

Muella M.T.A.H., de Paula, E.R., Kantor, I.J., Batista, I.S., Sobral, J.H.A, Abdu, M.A., Kintner, P.M., Groves, K.M., Smorigo, P.F., 2008. GPS L-band scintillations and ionospheric irregularity zonal drifts inferred at equatorial and low-latitude regions. Journal of Atmospheric and Solar-Terrestrial Physics, 70, 1261–1272.

Muella, M.T.A.H., Kherani, E.A., de Paula, E.R., Cerruti, A.P., Kintner, P.M., Kantor, I.J., Mitchell, C. N., Batista, I. S., Abdu, M. A., 2010. Scintillation producing Fresnel scale irregularities associated with the regions of steepest TEC gradients adjacent to the equatorial ionization anomaly. J. Geophys. Res., 115, A03301, doi:10.1029/2009JA014788.

Rino, C. L., 1979. A power law phase screen model for ionospheric scintillation. I-Weak Scatter., Radio Sci., 14, 1135–1145, 1147–1155.

Rishbeth, H., 1971. Polarization fields produced by winds in the equatorial F region. Planet. Space. Sci., 19, 357–369.

Spogli, L., Alfonsi, L., De Franceschi, G., Romano, V., Aquino, M.H.O., Dodson, A., 2009. Climatology of GPS ionospheric scintillations over high and mid-latitude European regions, Ann. Geo-phys., 27, 3429-3437.

Spogli, L., Alfonsi, L., De Franceschi, G., Romano, V., Aquino, M.H.O., Dodson, A., 2010. Climatology of GNSS ionospheric scintil-lation at high and mid latitudes under different solar activity conditions, Il Nuovo Cimento B, DOI 10.1393/ncb/i2010-10857-7.

Van Dierendonck, A. J., Klobuchar, J., and Hua, Q., 1993. Ionospheric scintillation monitoring using commercial single frequency C/A code receivers, in: ION GPS-93 Proceedings of the Sixth International Technical Meeting of the Satellite Division of the Institute of Navigation, Salt Lake City, USA, 22–24 September, 1333–1342.

Wernik, A. W., Liu, C.H., 1974. Ionospheric irregularities causing scintillations of GHz frequency radio signals. J. Atmos. Terr. Phys., 36, 871-879, 1974.

Young, E. R., Burke, W. J., Rich, F. J., Sagalyn, R. C., 1984. The distribution of topside spread F from in situ measurements by Defense Meteorological Satellite Program: F2 and F4, J. Geo- phys. Res., 89, 5565-5573.

Figure captions

Figure 1. Location of the CIGALA network receivers. In brackets, the number of receivers in the site. The orange line represents the position of the dip magnetic equator.

Figure 2. Map of S_4 percentage of occurrence above 0.25 in geographic coordinates for the period August to November 2011 (GPS L1). The orange line represents the position of the dip magnetic equator.

Figure 3. Map of σ_Φ percentage of occurrence above 0.25 radians in geo-graphic coordinates for the period August to November 2011 (GPS L1). The orange line represents the position of the dip magnetic equator.

Figure 4. Map of S_4 occurrence above 0.25 in latitude vs. UT for the period August to November 2011 (GPS L1).

Figure 5. Map of σ_Φ occurrence above 0.25 radians in latitude vs. UT for the period August to November 2011 (GPS L1).

Figure 6. Map of S_4 percentage of occurrence above 0.25 in geographic coordinates for the period August to November 2011 (GLONASS L1). The orange line represents the position of the dip magnetic equator.

Figure 7. Map of S_4 occurrence above 0.25 in latitude vs. UT for the period August to November 2011 (GLONASS L1).

Figure 8. Maps of S_4 occurrence above 0.25 in latitude vs. UT for the period August to November 2011 obtained by merging both GPS and GLONASS. Top plot is for L1, while bottom is for L2 data.

Figure 9. Map of the percentage of occurrence of S_4 above 0.1 radians for SCINTMON (Jan-Oct 2009, top plot) and PolaRxS PRU1+PRU2 (Feb-Oct 2011, bottom plot) in Geographic Latitude vs. Universal Time.

Images

Figure 1

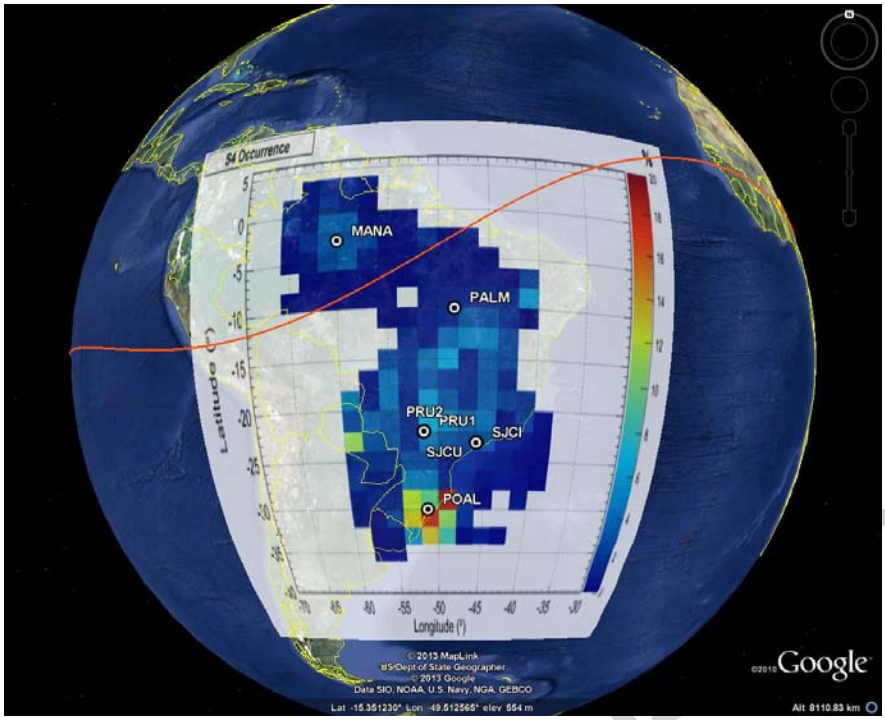

Figure 2.

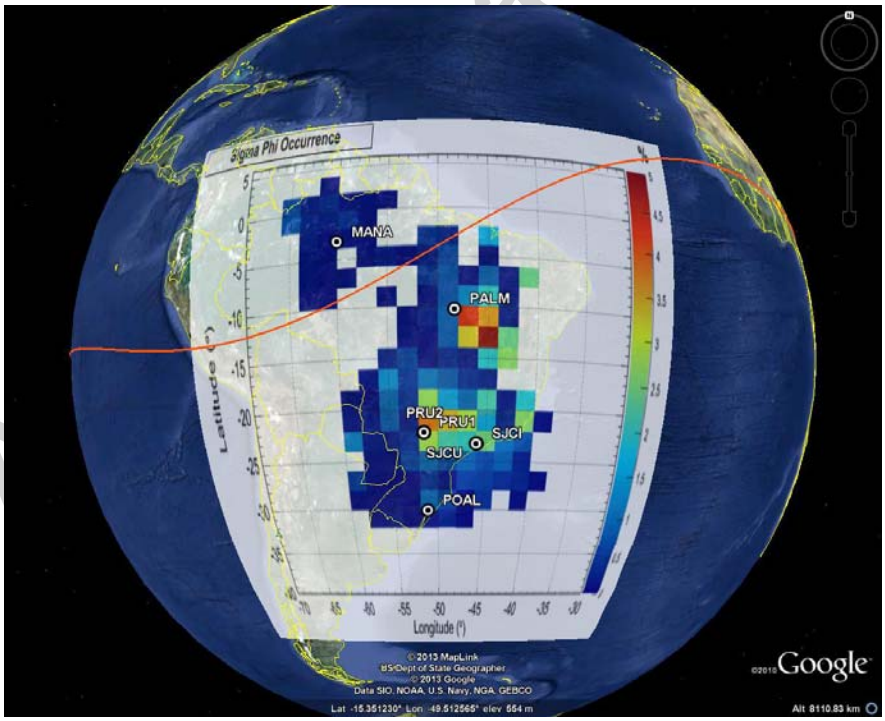

Figure 3.

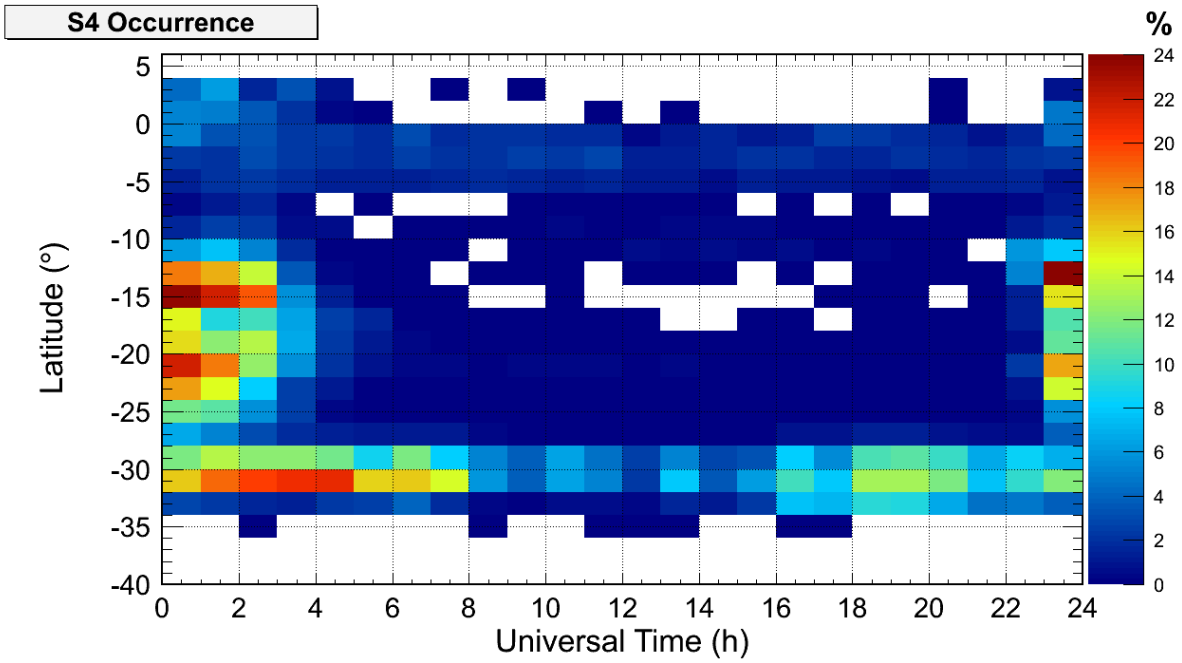

Figure 4.

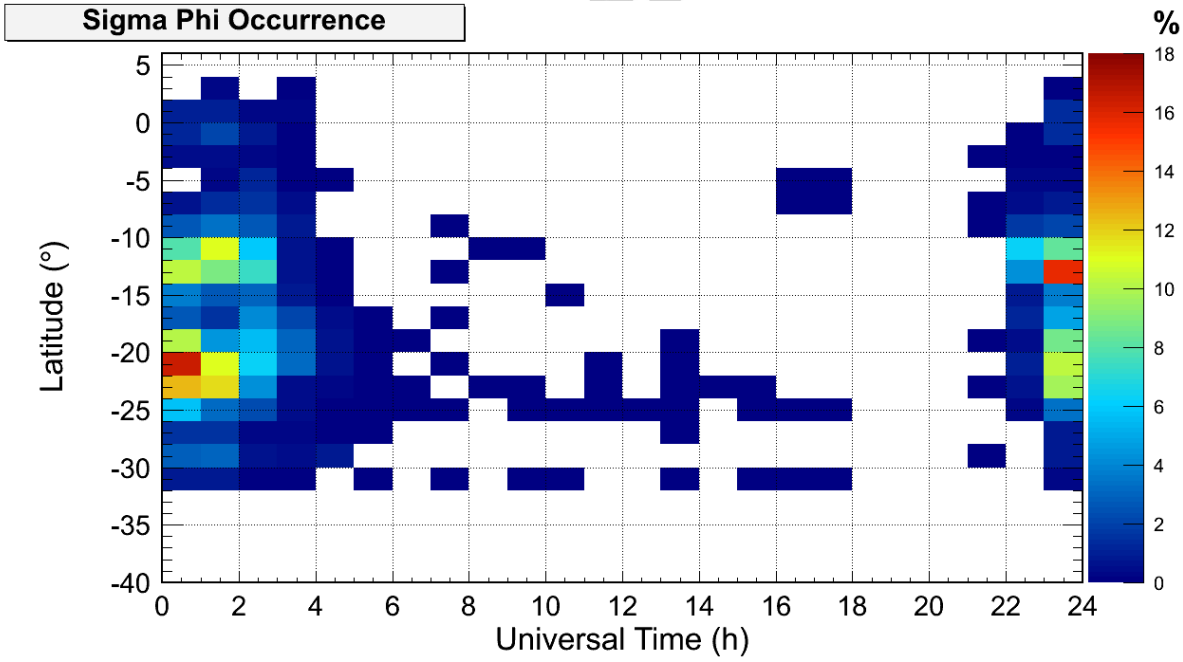

Figure 5.

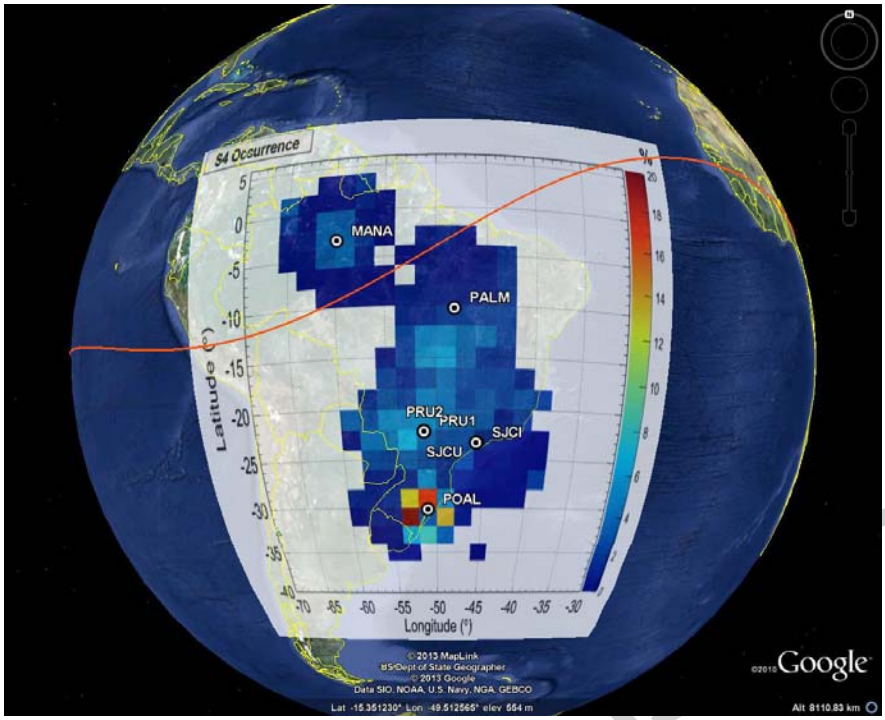

Figure 6.

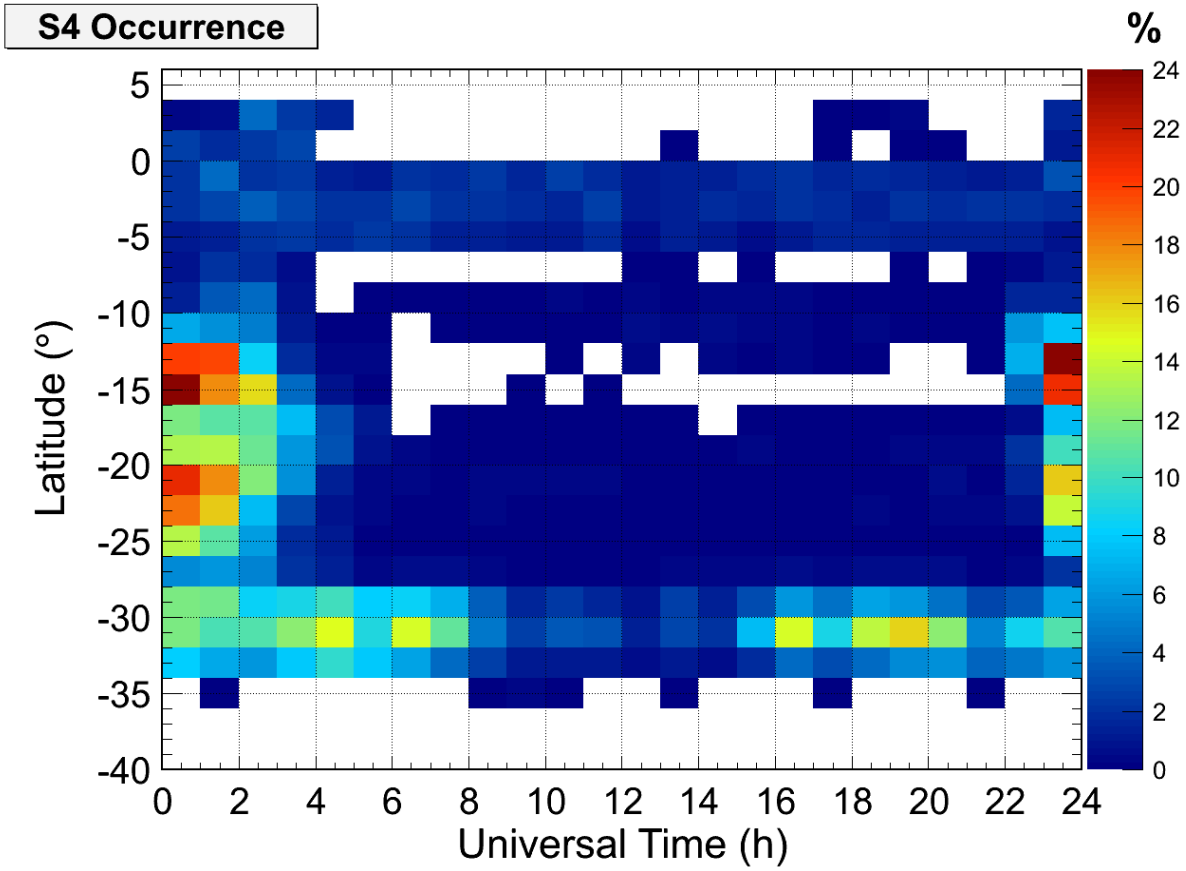

Figure 7.

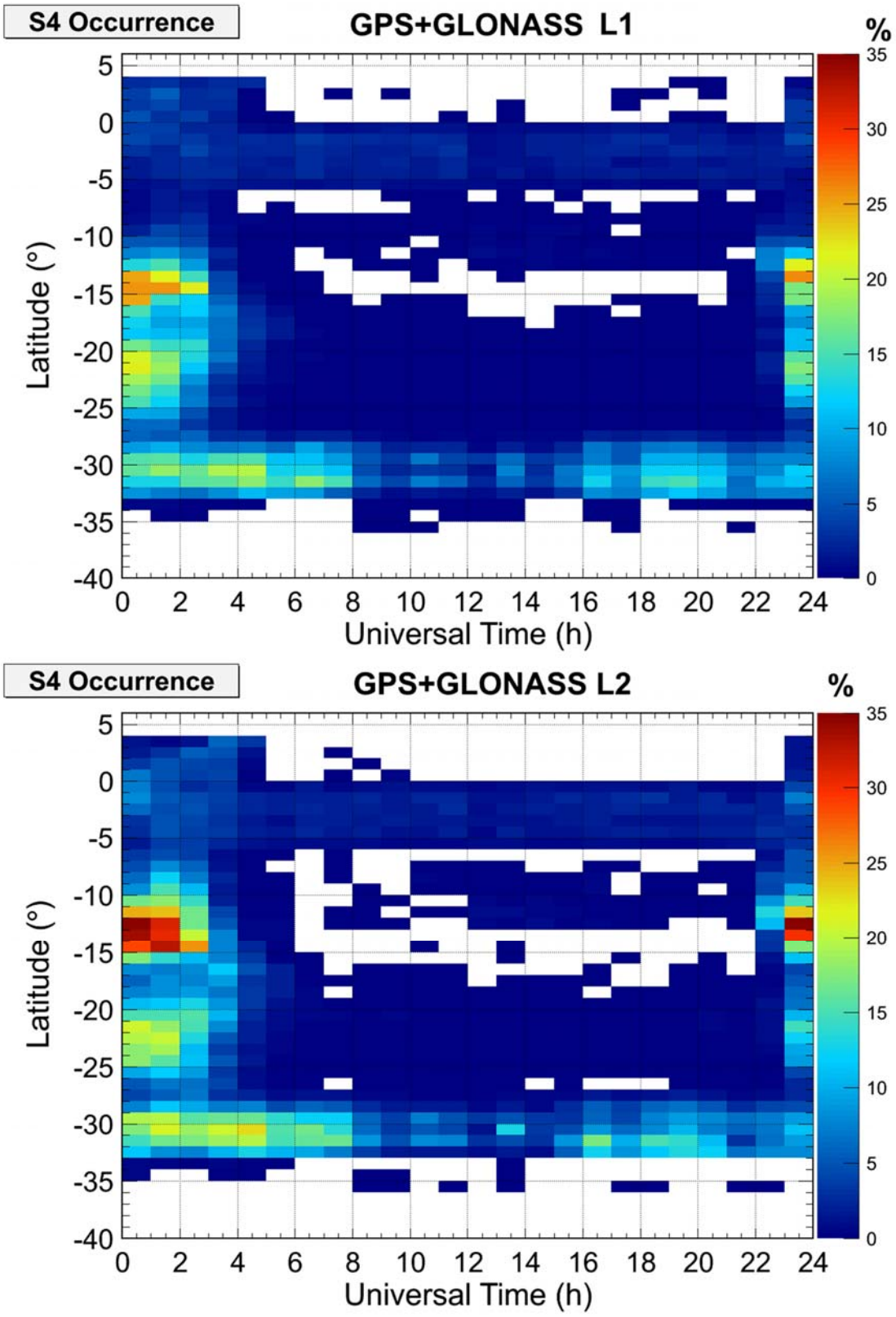
S4 Occurrence
GPS+GLONASS L1
%
35
30
25
20
15
10
5
0
Latitude (°)
5
0
-5
-10
-15
-20
-25
-30
-35
-40
0
2
4
6
8
10
12
14
16
18
20
22
24
Universal Time (h)
S4 Occurrence
GPS+GLONASS L2
%
Latitude (°)
Universal Time (h)

Figure 8.

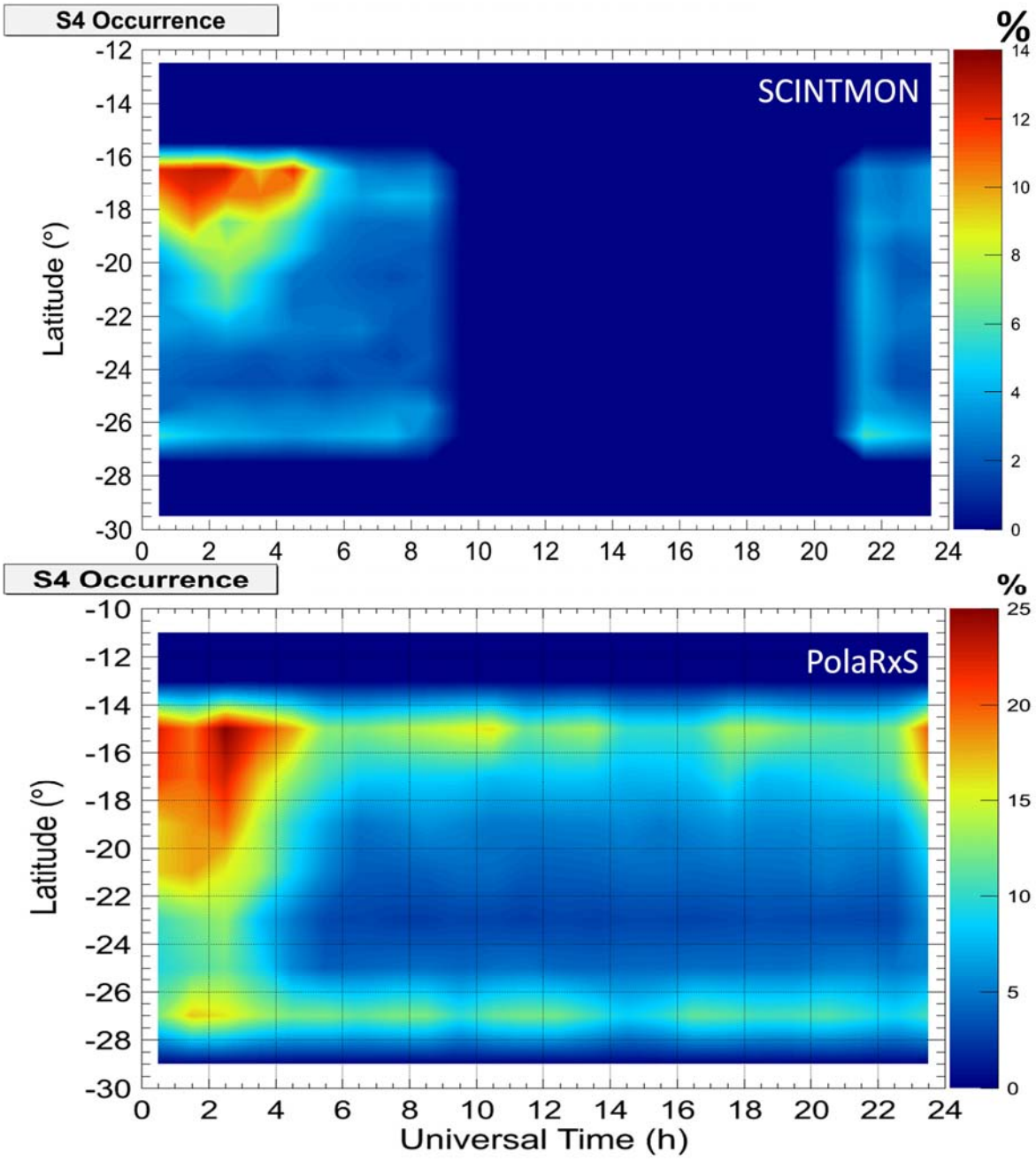
S4 Occurrence
SCINTMON
%
Latitude (°)
-12
-14
-16
-18
-20
-22
-24
-26
-28
-30
0
2
4
6
8
10
12
14
16
18
20
22
24
14
12
10
8
6
4
2
0
S4 Occurrence
PolaRxS
%
Latitude (°)
-10
-12
-14
-16
-18
-20
-22
-24
-26
-28
-30
Universal Time (h)
25
20
15
10
5
0

Figure 9

Tables

Table 1. List of all stations of the CIGALA network used in the present study.

ID	Location	Lat (°S)	Lon (°W)	Mag Lat (°S)	Installation date
PRU1	Presidente Prudente	22.120	51.409	12.73	09/02/2011
PRU2	Presidente Prudente	22.122	51.407	12.74	14/02/2011
PALM	Palmas	10.200	48.311	15.02	05/04/2011
SJCU	São José dos Campos	23.211	45.957	27.44	20/05/2011
SJCI	São José dos Campos	23.208	45.860	27.42	09/06/2011
MANA	Manaus	3.120	60.007	9.68	16/06/2011
POAL	Porto Alegre	30.074	51.120	34.96	04/07/2011

Table 2. Percentage of available days of data for each receiver in the considered period.

ID	Days of available data (%)
PRU1	48.4%
PRU2	95.1%
PALM	79.5%
SJCU	93.4%
SJCI	98.4%
MANA	63.9%
POAL	87.7%

Highlights

- Ionosphere over Brazil heavily affected by intense scintillation conditions
- Scintillation climatology on GPS and GLONASS (PolaRxS receiver, L1 and L2)
- Effect of Equatorial Anomaly and South Atlantic Anomaly in producing scintillation
- Comparative study with SCINTMON historical data shows agreement among the datasets